Rational Design of Plasmonic Nanostructures for Biomolecular Detection: Interplay between Theory and Experiments

Juan C. Fraire, Luis A. Pérez, and Eduardo A. Coronado*

INFIQC, Centro Laser de Ciencias Moleculares, Departamento de Fisicoquímica, Facultad de Ciencias Químicas, Universidad Nacional de Córdoba, Córdoba 5000, Argentina

ABSTRACT

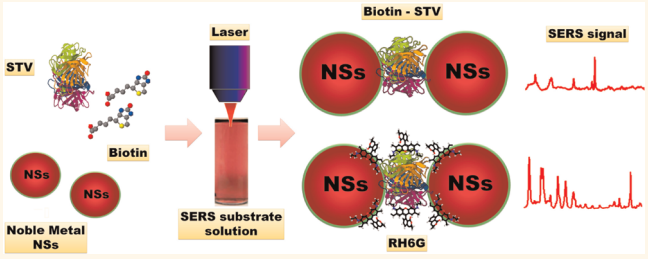

In this work, we report a simple strategy to obtain ultrasensitive SERS nanostructures by self-assembly and bioconjugation of Au nanospheres (NSs). Homodimer aggregates with an interparticle gap of around 8 nm are generated in aqueous dispersions by the highly specific molecular recognition of biotinylated Au NSs to streptavidin (STV), while random Au NS aggregates with a gap of 5 nm are formed in the absence of STV due to hydrogen bonding among biotinylated NSs. Both types of aggregates depict SERS analytical enhancement factors (AEF) of around 10^7 and the capability to detect biotin concentrations lower than 1×10^{-12} M. Quite interesting, the AEF for an external analyte, Rhodamine 6G (RH6G), using the dimer aggregates is 1 order of magnitude greater (10^5) than using random aggregates (around 10^4). The dependence on the wavelength and the differences of the AEF for Au random aggregates and dimers are rationalized with rigorous electrodynamic simulations. The dimers obtained afford a new type of an *in situ* self-calibrated and reliable SERS substrate where biotinylated molecules can selectively be "trapped" by STV and located in the nanogap enhanced plasmonic field. Using this concept, powerful molecular-recognition-based SERS assays can be carried out. The capability of the dimeric structures for analytical applications is demonstrated using SPR spectroscopy to detect biotinylated immunoglobulin G at very low concentrations.

KEYWORDS: plasmonics · nanoparticles · bioconjugation · SERS · sensing

Noble metal nanoparticle (NP) aggregates have long been recognized for their unique plasmonic properties, particularly their capability to couple to each other through near- and far-field interactions, giving rise to a variety of interesting optical phenomena, such as strongly confined and enhanced electromagnetic fields generated between the NPs, and to tune the plasmon resonance frequencies just by changing geometrical parameters, such as nanoparticle size,[1] shape,[1,2] crystal face,[3] surface roughness,[4] and particle−particle spacing.[5−10] These features allow us the possibility of making highly tunable SERS substrates, which is one of the most intense research areas of plasmonics. The synthesis and fabrication of SERS substrates have evolved from electrochemically roughened metal surfaces to random nanoparticle aggregates and finally to rationally designed nanostructures. Nowadays, our current ability to control the interparticle spacing and therefore to control the magnitude of the enhanced field in the gap is the subject of great interest and has led to many applications such as SERS, where the detection limit of a single molecule has been achieved.[11−19] Even top-down lithographic methods enable the fabrication of NPs on substrates with controlled geometry (NP morphology and interparticle spacing); they have the disadvantage that the minimum gap is limited by the electron beam wavelength (roughly tens of nanometers) and their fabrication is very expensive.

On the other hand, bottom-up approaches for constructing multidimensional nanoscale architectures have been successfully demonstrated using electrostatic interaction and hydrophobic interactions, *in situ* mineralization, covalent bonding, protein−protein interaction, and DNA hybridization.[20] Particularly, biomolecules show a great potential for functionalizing nanomaterials and constructing nanoscale architectures, due to their unique properties such as specificity, versatility, and multivalent nature. Additionally, they have the advantage that the distance and strength of the interaction

* Address correspondence to coronado@fcq.unc.edu.ar.

Received for review February 1, 2012 and accepted March 27, 2012.

Published online March 27, 2012
10.1021/nn300474p

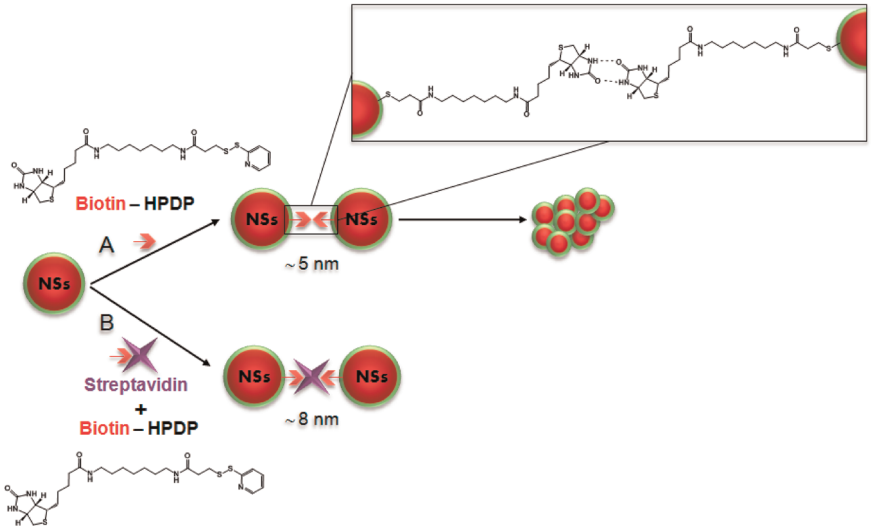

Scheme 1. Synthetic scheme showing the different nanogap engineering for the generation of nanosphere aggregates and dimers using biotin functionalization and bioconjugation through a biotin–Streptavidin system.[47] (A) Directional assembly of asymmetrically functionalized Au NSs into random structures with an interparticle gap around 5 nm, using molar ratios of 1:1 biotin/NSs. (B) Directional assembly of functionalized Au NSs by bioconjugation with streptavidin, leading to dimeric structures with an interparticle gap of 8 nm. The preferential formation of dimers depends on the molar ratios chosen (0.5:1:1 STV/biotin/NSs).

between the nanocomponents in the resulting nanostructures can be precisely controlled using biomolecule-directed strategies, which results in controlled nanogap SERS structures that would eventually allow single-molecule detection.[17] The most exciting feature of using these kinds of nanostructures in the emerging areas of biotechnology is the possibility to detect events and processes in biological systems with unprecedented levels of sensitivity and localization.[21–23] The usefulness of SERS for the detection of small molecules, nucleic acids, proteins, and cells, through direct enhancement of the Raman scattering of the analyte molecule or by indirectly detecting SERS-active nanoparticle tags bound to the analyte through specific affinity labels, is very well-known.[24–30]

Although many interesting SERS (bio)nanostructures have been reported, there still remains the great challenge of creating them in a facile, reproducible, and scalable manner in sufficient yield with near-optimal SERS activity. As already mentioned above, one of the most critical issues for achieving reproducible hot spots is to control the interparticle gap within a precision of a few nanometers. However, even with the importance this parameter plays in SERS measurements, there are only a few reports that aim to fabricate SERS aggregates with controlled gaps in solution,[17,31] with most being generated by electrostatic interaction with uncontrolled geometry of NP aggregation.[32,33]

The optimum SERS performance would be achieved if we are able not only to control the interparticle gap but also to place the analyte molecules precisely within these junctions of ultrahigh field enhancement. Biomolecules fulfill both requirements as they have the property of being specific linkers and also biorecognition agents able to preferentially place the target molecules within the hot spot. In this respect, some proteins are an excellent choice to generate SERS-active substrates since they are stable in aqueous solutions, can be readily manipulated and functionalized, and can also serve as linkers to construct nanoscale architectures with precise controlled gaps between NPs. The most popular biomolecular pairs using proteins for highly specific biomolecular recognition include the streptavidin–biotin,[34–40] antibody–antigen,[41–44] carbohydrate–selectin,[45] and peptide-based cross-linking.[46,47] To date, there are a wide variety of studies that have used the properties of the streptavidin (STV)–biotin interacting with NPs. For instance, it has been used to generate NP assemblies[34–40] and solid SERS substrates[48] and also to study the activity of proteins interacting with NPs.[49] Nevertheless, only a few of them tackle the problem of unveiling the optical properties of the assemblies generated, and to the best of our knowledge, there are no reports that exploit the special properties of these system to develop and rationalize the SERS behavior of thus nanostructures with controlled interparticle gaps in solution.

In this work, we report a simple synthetic strategy to obtain SERS structures by self-assembly of Au (NSs) in which the SERS-active region (*i.e.*, the gap between the nanoparticles) consists of metal–molecule–protein–molecule–metal junctions. In this gap, the biotin molecule acts as the SERS reporter and it is localized in the region of maximum enhancement of the hot spot. Two different types of SERS aggregates were generated using a stoichiometric control over the number of biotin molecules on the NSs surface and

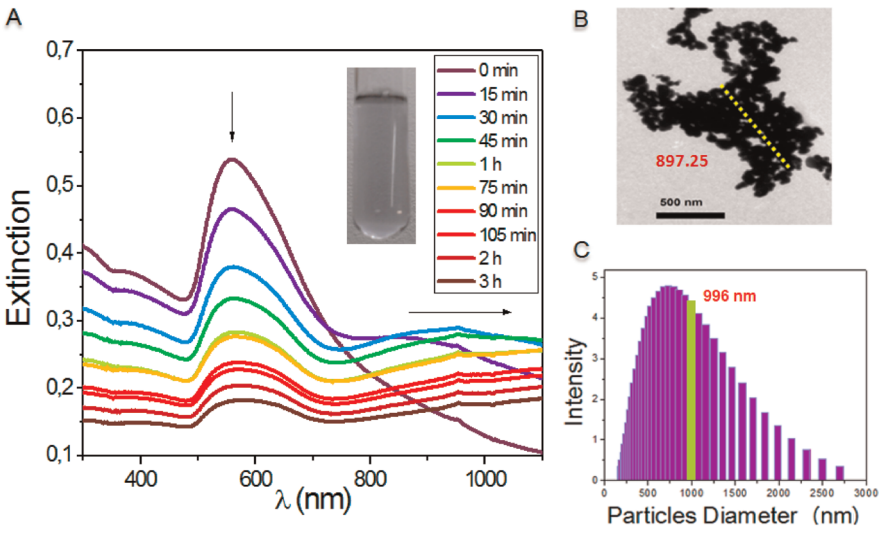

Figure 1. Optical and morphological characterization of random aggregates generated with 90 nm diameter Au NSs. (A) Extinction spectral evolution of the NS aggregation. The arrow at shorter wavelengths indicates the decrease of the extinction at the monomer resonant band, and the arrow at longer wavelengths denotes the red shift of the aggregate's collective resonance mode. (B) Representative TEM image of the tight compact random aggregates generated. (C) DLS scattering intensity as a function of the particle diameter (at 3 h of biotin addition). The vertical green line indicates the average size of the aggregate.

taking into account the fact that each STV protein can interact with a maximum of four biotin molecules.

On the one hand, we have produced NS dimers (one of the most efficient and widely used configurations in studies involving surface-enhanced phenomena, producing intense electromagnetic fields in the interstices of a reasonably simple structure) using the high specific biomolecular recognition and the strong interactions of the STV–biotin system, and on the other hand, we have also fabricated random aggregates, for comparative purposes, through the H-bond interactions between biotin molecules adsorbed onto the NSs. The central improvement here over previous reports, where such structures had been produced either purposely or inadvertently, is the development and design of an optimized nanoparticle linking protocol in which the SERS signal itself is used as the optimization parameter leading to a SERS substrate in aqueous phase of unprecedented intensity and reproducibility. The result is a quasi-isolatable, surface-functionalized material with uniform Raman response characteristics toward molecules that has been inherently positioned in the junction of the Au NSs.

In every case, in this work, two different approaches were used to generate the SERS substrates. The first one involves the biotinylation of Au NSs by the addition of "activated" biotin (molar ratio 1:1 biotin/NSs), which gets chemisorbed onto the surface of the NSs; the activation of biotin was performed by a thiol exchange reaction with mercaptoundecanoic acid (MUA), with a 1:10 biotin/MUA ratio. In this first procedure, it is apparent (see below) that, on average, there was one biotin per nanoparticle ([biotin] = 2.20×10^{-12} M), and that the interaction of the biotinylated NSs leads to the formation of random aggregates through H-bonds between biotins, with an interparticle gap of around 5 nm (Scheme 1A). The second approach used was to add simultaneously biotin and STV, with an average concentration of one biotin molecule per NS and one STV molecule every two NSs. In this case, as illustrated in Scheme 1B (further corroborated by TEM images, dynamic light scattering (DLS), UV–vis spectroscopy, and electrodynamics modeling), the formation of dimers is induced by linking biotinylated NSs mediated by the STV molecule. In this case, the formation of NS dimers with a gap of around 8 nm is generated.

RESULTS AND DISCUSSION

Far-Field Optical and Morphological Characterization of the Substrates. Although we have performed experiments using Au NSs of different diameters, only the morphological and optical characterization corresponding to 90 nm diameter Au NSs will be presented here. The SERS substrates formed with 36 nm diameter Au NSs and their morphological and optical characterization are given in the Supporting Information.

Let us first discuss the far-field optical behavior obtained after biotinylation of Au NSs. The spectral changes at different times after the addition of biotin (final concentration of 2.20×10^{-12} M) are shown in Figure 1A. The main feature to be noticed is the appearance of a second band at longer wavelengths which gradually red shifts and broadness as time elapses. This optical behavior is indicative of NP aggregation, as it was further confirmed by TEM analysis and by DLS experiments after 3 h of reaction time. The DLS results indicate that Au NS aggregates are formed

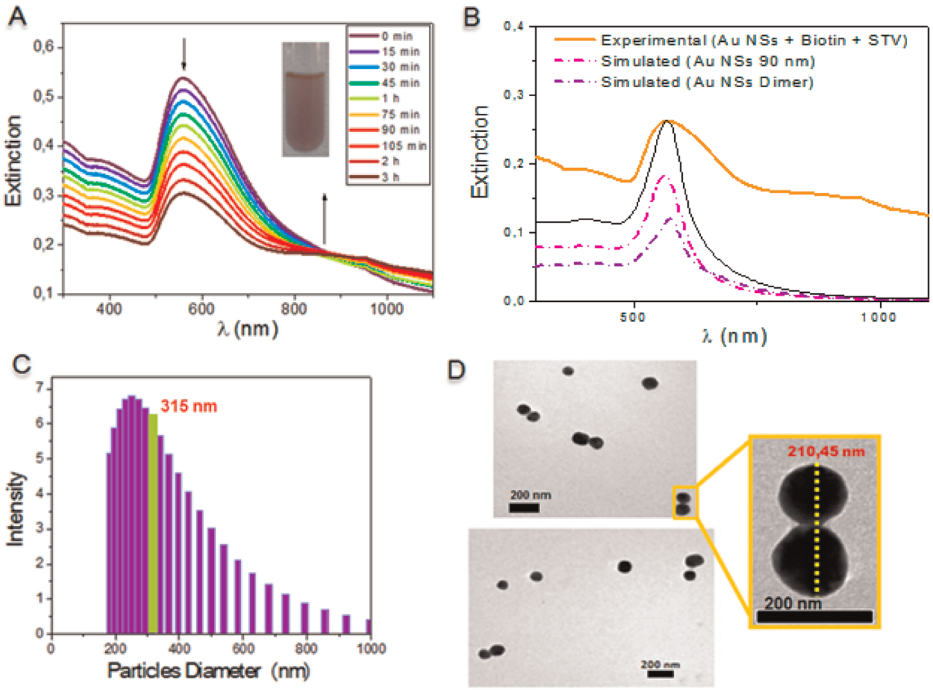

Figure 2. Optical and morphological characterization of dimers generated with 90 nm diameter Au NSs. (A) Extinction spectral evolution of the NS aggregation. The arrow at shorter wavelengths indicates the decrease of the extinction at the monomer resonant band, and the arrow at longer wavelengths denotes the presence of a minor aggregate collective resonance mode. (B) Correlation of the experimental spectrum (3 h) and the simulated spectra using GMM for a 90 nm Au NS dimer using a gap between particles of 8 nm (averaged over 8 different orientations), together with the spectrum of an isolated 90 nm Au NS. The solid black line is the result of considering the calculated spectrum of both the monomer and the dimer. (C) DLS scattering intensity as a function of the particle diameter (at 3 h of biotin and STV addition). The vertical green line indicates the average size of the dimer. (D) Representative TEM image of the dimers generated.

with an average size of 996 nm (see DLS histogram in Figure 1C), while the TEM images show that these aggregates seem to be tight compact clusters, formed during a random agglomeration process (Figure 1B). The band in the extinction spectrum which suffers the most significant red shift at longer wavelengths will be denoted hereafter as "collective mode of the aggregate" as it is the one whose red shift clearly denotes NP aggregation.

The results obtained by the simultaneous addition of biotin and STV, to reach a final concentration of 2.44×10^{-12} and 1.10×10^{-12} M, respectively, are significantly different. The spectral evolution in the early stages of reaction does not depict the presence of a secondary band, just only a minor increase in the extinction red-shifted and broadening with respect to the plasmon resonance band of isolated Au NSs that could be assigned to a minor agglomeration process (Figure 2A). Considering the simulated spectrum of a 90 nm Au NS dimer with a gap between particles of 8 nm and the simulated spectrum of a 90 nm Au NS monomer (both spectra simulated using GMM theory), the experimental spectrum could be interpreted as the superposition of both (see Figure 2B). Details of how to calculate the far-field as well as the near-field properties of NS aggregates can be found elsewhere.[50−52] This good correlation between theory and experiments was a first indication of the formation of NS dimers. A more conclusive evidence of dimer formation was obtained by the TEM and DLS morphological characterization (Figure 2C,D). DLS measurements indicate that controlled aggregates (dimers) of Au NSs are formed with an average size of 315 nm (see DLS histogram), while the TEM images reveal that the nanostructures obtained were mostly spheroidal Au dimers (45%) together with some monomers. It should be noticed that the intensities of DLS signals shown in Figure 2C are in signal intensity units; therefore, they are proportional to the scattering efficiency of the clusters. As the scattering cross section scales in the quasistatic limit with the sixth power of size, larger clusters will have very high scattering intensities even if their concentration is very low compared with that of the smaller clusters (*i.e.*, a cluster being 10 times greater in size will have a million times greater scattering cross section).[53] Taking into account the above points and considering the relative scattering intensities of the larger cluster in the tail of the DLS histogram of Figure 2C, it can be concluded that the presence of large clusters is negligible compared to small nanostructures as monomers and dimers. This analysis explains also the fact that in the TEM images analyzed we did not observed any cluster of larger size.

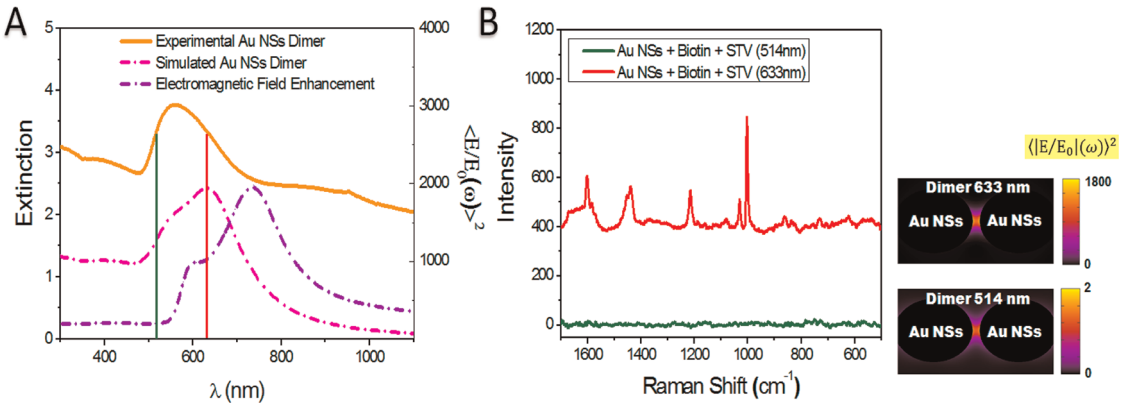

Figure 3. Near-field optical characterization of 90 nm Au NS dimers. (A) Comparison between experimental extinction and calculated extinction and enhancement spectrum at different wavelengths for a 90 nm diameter Au NS dimer with a gap between particles of 8 nm. Vertical lines indicate the excitation wavelengths used to obtain the SERS spectra (right panel). (B) SERS spectra obtained by irradiation at 514 and 633 nm, and near-field GMM calculations of the enhanced field at the two different wavelengths chosen for the acquisition of the SERS spectra; the color scale bar corresponds to the square power of the enhanced electric field.

Although it should be more appropriate to use near spheroidal shapes, the approach to consider spherical NPs to model the far- and near-field optical properties was remarkably good as it was able to describe the main optical features observed in the experiments, as mentioned above. Even the gap between NPs (8 nm) cannot be confirmed by TEM analysis, a free space between the particles cannot be totally ruled out. As the NSs are in fact faceted, it is quite possible that there is a slight overlap of their TEM images projected on the substrate plane,[54] making it impossible to determine the interparticle distance. In addition, it should be noticed that the distances under vacuum should be shorter than that of particles in solution.[55] Further evidence that the gap produced between NS dimers is indeed around 8 nm was also tested by producing dimers of 36 nm diameter Au NSs. As shown in the Supporting Information, the extinction spectra of these structures (Figure S3 in the Supporting Information) are in agreement with electrodynamics simulation only if the same interparticle gap (8 nm) is assumed.

The generation of dimeric nanostructures is mainly controlled by the stoichiometric ratio between biotin and streptavidin. The great affinity of these two molecules is reflected by the high value of the association constant of the streptavidin–biotin pair, which is in the range between 3.0×10^6 and 4.5×10^7 M^{-1} s^{-1}.[56] Therefore, the reaction between streptavidin and biotin may occur orders of magnitudes faster than NP functionalization and dimerization, and as a consequence, the stoichiometry of these two reactants is what actually controls the formation of dimers or small clusters.

On the other hand, in the absence of the protein, the functionalization and aggregation process occur without the kinetic control of the streptavidin–biotin reaction. In this case, the stoichiometric ratio between biotin and NPs does not ensure the formation of dimers probably because the functionalization process as well as the formation of hydrogen bonding competes at similar rates, and the mixing of the reactants (NPs and biotin) does not exert any control on the amount of biotin molecules per nanoparticles. This feature gives rise to any control on the directionality of dimer formation and therefore to the generation of clusters of larger size.

Near-Field Optical Characterization and Sensing Performance of the Aggregates. As discussed above, both biotin and biotin–STV systems induce aggregation with a controlled separation between two or more Au NSs. It is well-known that the molecules in such nanogaps should experience an intense enhancement of the electromagnetic field, which is confined within the gap (hot spot), and is responsible for the SERS effect. Since biotin is Raman-active[46] and is located at both sides of the gap, where the hot spots have the maximum values of enhancement (see near-field calculations below), the NS system is a good candidate for a self-calibrated SERS substrate. This is so because the intensity of the SERS signals from biotin can be used to determine the magnitude of the maximum SERS intensity of a dimer. For 36 nm diameter Au NS random aggregates and dimers, no SERS signal was detected from biotin using a 2.44 pM concentration due to the small field enhancement within the gap at the irradiation wavelengths (514 and 633 nm) used in the experiments (see Figure S4 of the Supporting Information). These results are in contrast with the SERS enhancement obtained using 90 nm diameter Au spheres where significantly higher enhancement values are induced according to our GMM simulation. For the 90 nm Au NS dimers characterized previously, the longitudinal mode is at 635 nm and the aggregates' collective resonant mode is in the range of 650–850 nm, which was suitable for resonant excitation by 633 nm light (note that the spectral positions of

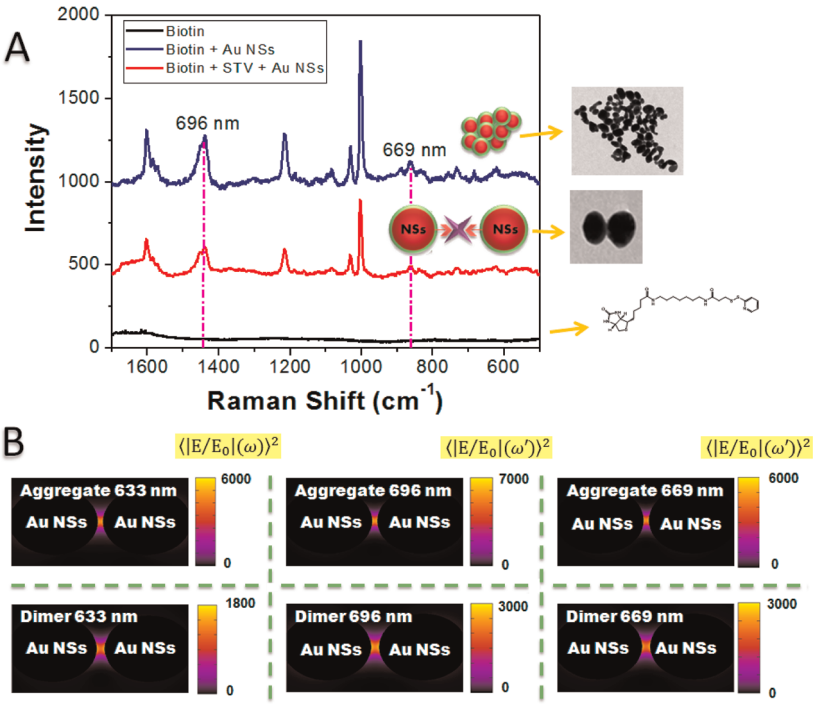

Figure 4. Near-field optical characterization of 90 nm Au NS substrates: random aggregates and dimers. (A) SERS spectra for colloidal solutions of the random aggregates and dimers, and the Raman spectrum of a picomolar solution of biotin. The two wavelengths of the Stokes signals for biotin (696 and 669 nm) are indicated by the vertical lines. (B) Near-field GMM calculations of the enhanced field for the substrates at the incident wavelength (633 nm), and the calculations at the wavelengths of the Stokes signals for biotin chosen, necessary for the calculation of theoretical enhancements (see text).

the aggregates change in time but the longitudinal mode of the dimer does not). Figure 3 compares the huge enhancement in the SERS spectrum for the dimer of 90 nm Au NSs irradiating in resonance at 633 nm, with the small enhancements obtained at 514 nm. It is worthwhile to appreciate that the signal that could be assigned only to the STV molecule is a shoulder at 1646−1675 cm^{-1} (R−N−C(O)−R amide stretching), which is absent in the SERS spectrum of biotin (see Figure 4B, red line). The other vibrational modes of the protein are almost at the same wavenumbers than the ones corresponding to biotin, but as the protein is in a region of smaller field enhancement, these modes are by far of lower intensity. In order to explain this behavior, we performed near-field calculations for these dimers at the two different wavelengths, considering the polarization of the electric field along the dimer axis. Figure 3B clearly shows that the maximum enhancement, $\Gamma(\omega) = (|E/E_0|(\omega))^2$, is achieved at 633 nm, which corresponds to the longitudinal dipolar mode of dimers. Excitation of the transversal mode at 514 nm generates a negligible field enhancement. These near-field calculations agree quite well with the experimental results and reveal that the maximum enhancement is localized in the gap near the NS surface.

Comparing the simulation of the dimer extinction spectrum with the enhancement calculation at each wavelength reveals that there is a considerable red shift of the enhancement with respect to the maximum of the extinction spectra (see Figure 3A, pink and violet lines). Although the enhancement is very low at 514 nm, the extinction is significant at this wavelength. This red shift of the near-field optical properties with respect of the far-field optical properties can be explained considering that the imaginary part of the dielectric constant of Au has a greater value at this shorter wavelength (514 nm) than at 633 nm and, therefore, a major damping. As a consequence, the quality factor should be lower and the enhancement very small.[57]

In Figure 4A, we compare the SERS spectra obtained for random and dimer colloidal solutions for excitation at 633 nm. At first glance, as the interparticle distance in the aggregates is shorter (5 nm) than in the dimers (8 nm), a strong coupling of plasmons should induce a greater enhancement. Nevertheless, the SERS signals for the random aggregates are only slightly higher. This observation can be rationalized theoretically by performing near-field calculations of the electric field enhancement using GMM theory considering that, for the random aggregates, the most significant contribution comes from dimers with 5 nm interparticle gaps. Although the calculated enhancement $\Gamma(\omega)^2$ at 633 nm (Figure 4B) is almost 10 times greater for random aggregates than dimers, the experimental spectra depict a less significant difference. As should be discussed later, these lower values can be explained by a collective effect that should be explained below.

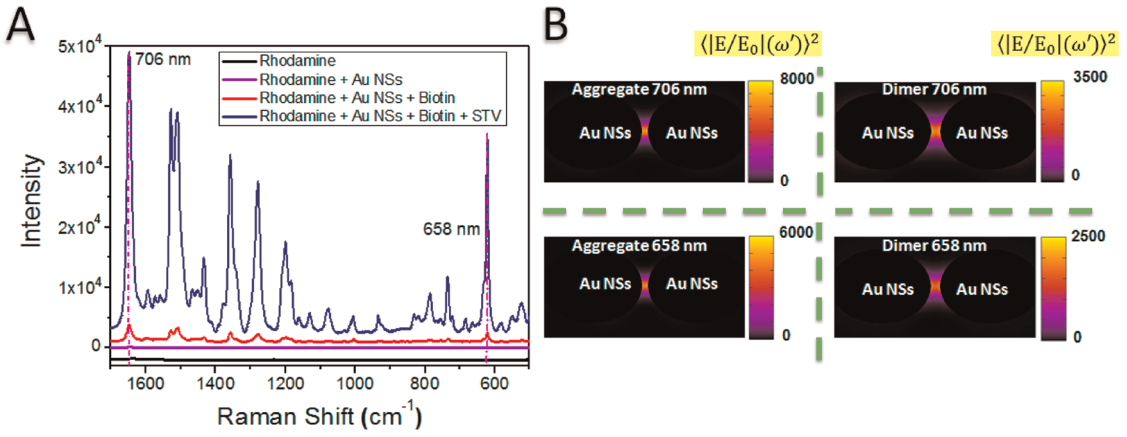

Figure 5. Optical response of Rhodamine 6G in the presence of SERS substrates of 90 nm Au NSs. (A) SERS spectra of the colloidal solution of the random aggregates and the dimers containing Rhodamine 6G, and a solution of 1×10^{-7} M Rhodamine. Also shown are the two wavelengths of the Stokes signals for Rhodamine (706 and 658 nm). (B) Near-field GMM calculations at the wavelengths of the Stokes signals for biotin chosen, necessary for the calculation of theoretical enhancements irradiating at 633 nm (see text).

Besides the plasmonic properties of the dimers and the aggregates that arise from bioconjugation, which allow us to detect picomolar solutions of biotin, their optical properties can also be harnessed for sensing applications. As a probe of concept, we have used an external molecular probe such as the Rhodamine 6G (RH6G) dye to compare the SERS performance of Au NS random aggregates and dimers. Figure 5A shows the SERS spectra for colloidal solutions of 90 nm Au NS aggregates containing 10^{-7} M RH6G. As expected, there is a significant enhancement in the signals for the dye in the presence of the aggregates. In particular, the highest SERS intensity of RH6G is achieved for the dimeric substrates. This feature could be due to a preferential interaction of this cationic dye with the protein (STV), and therefore, the dye has a greater probability of experiencing an enhanced field in the hot spot region. Figure 5B shows the near-field calculations at two different Stokes wavelengths of the dye, used for estimating the theoretical enhancement (see below). The fact that the highest intensities of RH6G are achieved with dimeric aggregates than with random aggregates constitutes further evidence that there is a preferential interaction of RH6G with the protein (STV) which generates preferential localization in the regions of high enhancement.

Now, we will give a quantitative assessment of our results by comparing the experimental and the theoretical enhancement values.

The SERS enhancement factor, for many applications, is related to the simple question of how much stronger is the SERS signal produced by an analyte at a given normal mode compared to the normal Raman signal of this mode in a given experimental condition. For analytical chemistry applications, especially those involving substrates in solution, it is suitable to use the so-called analytic enhancement factor (AEF), which is defined as the ratio of the intensity of the SERS signal (I_{SERS}) of a given mode and the intensity of the Raman signal (I_{SR}) of the same mode for a given analyte, both normalized with the respective analyte concentration (C):[58]

$$\mathrm{AEF} = \frac{I_{SERS}/C_{SERS}}{I_{SR}/C_{SR}} \quad (1)$$

This is valid as long as the experimental conditions for measuring the Raman spectrum and SERS spectrum are the same (wavelength and power of the laser, microscope objective or lens, spectrometer, *etc.*).

From the theoretical point of view, the main mechanism that produces the SERS effect is the electromagnetic one. Therefore, the enhancements of the SERS signals are proportional to the so-called "electromagnetic field enhancement factor", EFEF, given by

$$\mathrm{EFEF} = \langle (|\Gamma|(\omega))(|\Gamma|(\omega')) \rangle \quad (2)$$

$$\langle |\Gamma|(\omega) \rangle = \left\langle \left(\left| \frac{E}{E_0} \right| (\omega) \right) \right\rangle^2 \quad (3)$$

$$\langle |\Gamma|(\omega') \rangle = \left\langle \left(\left| \frac{E}{E_0} \right| (\omega') \right) \right\rangle^2 \quad (4)$$

where $|\Gamma|(\omega)$ is the square of the enhanced electric field generated at the frequency of the incident radiation (ω) and $|\Gamma|(\omega')$ is the square of the enhanced electric field generated at a particular Stokes frequency (ω').[59]

Using these definitions, the EFEF calculated according to eq 2 will be compared with the AEF given by eq 1 for Au aggregates and dimers. The comparison was performed for the Stokes signals of biotin at λ = 696 and 669 nm (highlighted by the vertical lines in Figure 3C) and for RH6G at λ = 706 and 658 nm (highlighted by the vertical lines in Figure 4A). The EFEF was calculated for the maximum enhancement obtained in the near-field calculations of the

TABLE 1. Experimental and Theoretical Enhancement Factors in 90 nm Au NS SERS Substrates in Aqueous Solution for the Detection of Biotin and Rhodamine 6G[a]

composition	c/ω (nm)	analyte	$C_{analyte}$ (M)	Raman (counts)	ν (cm^{-1})	AEF	c/ω' (nm)	$\|\Gamma\|^2_{max}$
biotin	633	biotin	9.25×10^{-6}	42	1439			
biotin + NSs	633	biotin	2.44×10^{-12}	292	1440	2.64×10^{7}	696	2.45×10^{7}
biotin + NSs + STV	633	biotin	2.44×10^{-12}	169	1440	1.53×10^{7}	696	4.94×10^{6}
biotin	633	biotin	9.25×10^{-6}	38	868			
biotin + NSs	633	biotin	2.44×10^{-12}	110	863	1.11×10^{7}	669	2.10×10^{7}
biotin + NSs + STV	633	biotin	2.44×10^{-12}	64	863	6.38×10^{6}	669	3.82×10^{6}
RH6G	633	RH6G	1×10^{-3}	713	1652			
RH6G + biotin + NSs	633	RH6G	1×10^{-7}	2178	1647	3.05×10^{4}	706	2.80×10^{7}
RH6G + biotin + NSs + STV	633	RH6G	1×10^{-7}	17186	1647	2.41×10^{5}	706	5.38×10^{6}
RH6G	633	RH6G	1×10^{-3}	1249	613			
RH6G + biotin + NSs	633	RH6G	1×10^{-7}	1537	621	1.23×10^{4}	658	2.10×10^{7}
RH6G + biotin + NSs + STV	633	RH6G	1×10^{-7}	12151	621	9.73×10^{4}	658	3.29×10^{6}

[a] RH6G = Rhodamine 6G; AEF = analytic enhancement factor; $|\Gamma|^2_{max}$ = theoretical enhancement considering the square power of the enhanced field at the incident frequency (ω) multiplied by the square power of the enhanced field at a Stokes frequency (ω').

aggregates at the incident frequency, multiplied by the maximum enhancement calculated at a Stokes frequency for every cluster geometry.

The results for the different 90 nm Au NS aggregates are shown in Table 1. There is an excellent correlation between the AEF and the EFEF ($\times 10^7$), considering the biotin signals in all substrates (random aggregates and dimers), for the two Stokes modes (696 and 669 nm). These values are on the order of the biggest AEF for self-calibrated SERS substrates in solution.[34] There are two features to be mentioned. First, a comparison of the theoretical maximum enhancement of the random aggregates with that of the dimers for the same Stokes band reveals that the AEF should be a factor of 10 greater for random aggregates than for dimers. However, the experimental AEF is a factor of 2 or 4 greater for random aggregates. This result could be explained considering that, in the calculations for the aggregates, we have considered dimers with a smaller interparticle distance (5 nm), which indeed should produce a greater enhancement. This calculation, however, constitutes an upper bound to the "real enhancement" experienced by the aggregates since not all of the gaps within the particles in the aggregates would contribute to the SERS enhancements. In fact, it is reasonable to think that the gaps of the aggregates located in the "core" will be "shadowed" by the NPs in the external sides of the aggregates. Therefore, there should be a lower effective number of hot spots in the random aggregates than in dimers, for the same NP concentration. A simulation of the near-field enhancement produced in a 90 nm Au NS cluster (given in the Supporting Information, Figure S5) demonstrates that this is indeed the explanation since there is clear evidence of the anisotropy of the field distribution within the aggregate, with the field in the inner side of the aggregate being weaker than that produced in the outer shell of the aggregate. Another important issue to discuss is the difference in the AEF for the two Stokes frequencies (ω'). For Au NS random or dimers, the AEF is greater for the lowest ω' (highest wavelength). This result is explained considering that the EFEF for each wavelength is red-shifted with respect to the extinction spectra, being stronger for the lowest wavelengths (see Figure 3A, violet line). For RH6G as the external analyte, there are significant differences between the maximum of the EFEF and the experimental AEF (2 orders of magnitude). This fact could be rationalized considering that RH6G could be located in nonspecific sites and therefore should experience a lower mean field than biotin, which is mainly in the region of maximum enhanced field between the NSs. Nevertheless, the AEF achieved in this case (10^5) is within the magnitude of that obtained for external analytes in colloidal dispersion having more complex synthetic and/or irreproducible performance.[58,60]

Surface Plasmon Sensing Using Dimeric Bioconjugated Au NSs. The experiments shown above demonstrate the potential of these aggregates as useful SERS devices for analytical assays. Moreover, the presence of two vacant sites for interaction with biotin in the dimers has the potential of using these aggregates for biomolecular detection. In this section, we will test the performance of these dimeric structures to sense biotinylated immunoglobulin G (IgG) using localized surface plasmon resonance (LSPR) spectroscopy. For this purpose, we have followed the change of the extinction spectra of these mostly dimeric structures after the addition of picomolar concentrations of biotinylated IgG using dimer/IgG concentration ratios of 1:0.5, 1:1, and 1:2 (with the IgG concentration being 0.61×10^{-12}, 1.22×10^{-12}, and 2.44×10^{-12} M, respectively). As depicted in Figure 6, there is clear evidence of agglomeration by the appearance of a plasmon band at longer wavelengths after only 10 min of the addition of IgG. This agglomeration can be explained considering that the IgG molecules used have multiple biotinylated sites,

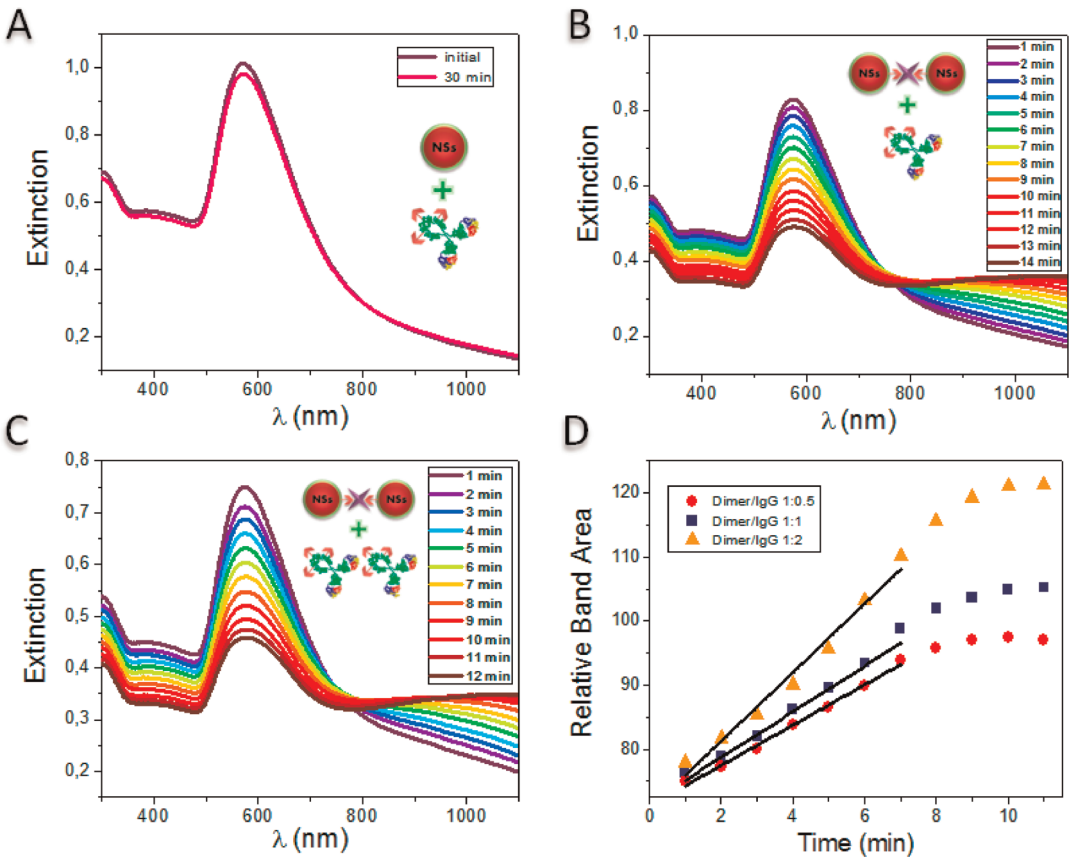

Figure 6. Immunoglobulin (IgG) detection through SPR shifts in Au dimer agglomeration. (A) Extinction spectral evolution for Au NPs in the presence of an excess of biotinylated IgG. (B) Extinction spectral evolution for Au dimers in the presence of biotinylated IgG (dimer/IgG 1:1). (C) Extinction spectral evolution for Au dimers in the presence of biotinylated IgG (dimer/IgG 1:2). The arrows at shorter wavelengths indicate the decrease of the extinction at the monomer resonant band, and the arrow at longer wavelengths denotes the red shift of the aggregates' collective resonance mode. (D) Monitoring the increase of the collective resonance mode area as a function of time for three different concentrations of IgG.

able to bioconjugate with the non-occupied biotin receptor sites of the streptavidin (acting as the bridge in the dimeric structures). As a test that this is indeed the case, we have carried out experiments adding a micromolar concentration of IgG to a Au NP colloidal solution, and we did not observed any spectral change (only a minor depletion of the extinction maximum after half an hour).

A plot of the area of the longer wavelength band of the extinction spectra, that is, between 760 (isosbestic point) and 1100 nm, *versus* time gives a linear relationship with a slope that depends on the initial IgG concentration (Figure 6D). It is evident that the wide range of biotinylated biomolecules available for detection opens up the exciting possibility of solution-based selective self-calibrated SERS biosensors (biotin signals of the aggregates allow one to check the reproducibility) and opens opportunities in the synthesis of specific nanostructures for materials science and biodetection applications. Moreover, the synthetic strategy presented can be scalable in order to generate SERS-active substrates and nanoprobes with a very precise control over the gap in the nanometer scale and with high reproducibility.

CONCLUSIONS

Self-calibrated SERS dimeric Au nanostructures have been successfully prepared by bioconjugation using streptavidin and biotin molecules, locating these molecules within the gap of 90 nm diameter Au NSs with strict stoichiometric control. We have shown that strong and reproducible SERS signals, with enhancements factors around 10^7, can be obtained for these dimeric substrates for the biotin molecule acting as a SERS reporter, which means that whenever a dimer has been synthesized, a rough determination of the SERS enhancement allows us to estimate the maximum enhancement that can be achieved (*i.e.*, they are self-calibrated substrates).

The SERS performance of these bioconjugated dimers has been compared with random aggregates, demonstrating that both types of aggregates have almost the same AEF, being only slighter higher for the random aggregates. However, even it should be expected that both types of substrates generate high enhancements in the SERS signals for the local reporter; the first type has the advantage of being more "stable" and to have specific structural geometry. The

"stability" is associated with the different plasmon behavior of both types of substrates; while the longitudinal dimer mode remains almost at the same wavelength, the aggregate mode at longer wavelength red shifts in time.

The excellent agreement between modeling and experiments allowed us to explain the near- and far-field plasmonic behavior of these aggregates. The good correlation between the simulated and the experimental extinction spectra for dimers of Au NSs of different size indicates that the interparticle distances proposed should be correct. Moreover, the simulation of the near-field response of these dimeric aggregates allows us to explain the differences in the AEF for each Stokes frequency, in terms of plasmon damping effects that give a red shift of the extinction spectra with respect to the variation of the EFEF with wavelength.

Finally, it has been demonstrated that these bioconjugated substrates can be further modified by other biotinylated biomolecules (immunoglobulins, specific proteins, *etc.*) having the potential to be used for both analytical purposes and biolabeling probes with ultrahigh sensitivity. Further work on this line is under development in our laboratories.

Certainly, the detection sensitivity of the SERS signals for external analytes (other than those located within the gap, *i.e.*, biotin and streptavidin) will be dependent upon the relative Raman cross sections of the normal modes of the molecules inside the hot spot and the corresponding normal modes of the external molecules to be detected by SERS. In this respect, we demonstrate that the detection of an external analyte, such as Rhodamine 6G, could be performed at very low concentrations (in our experiments around 10^{-7} M), but actually this concentration can be even lower as the SERS signals are at this concentration high enough to be able to reduce at least 1 or 2 orders of magnitude this detection limit (*i.e.*, it would be possible to detect nanomolar concentrations). We did not attempt to detect by SERS an external analyte able to be specifically linked to the other two sites of streptavidin; this issue would be the subject of future work. However, we take advantage of the changes of the LSPR spectra induced by their aggregation through bioconjugation and demonstrate that subpicomolar detection of biotinylated proteins such as IgG is possible.

MATERIALS AND METHODS

Materials. The following materials were used as obtained: $HAuCl_4$ (Carlo Erba); sodium citrate (Mallinckrodt); Rhodamine 6G (Exciton); EZ-Link biotin-HPDP (Pierce); streptavidin (Invitrogen); anti-mouse IgG biotin (Sigma).

Au Nanosphere Synthesis. The synthesis of gold nanoparticles was performed using the Turkevich method, which is based in the reduction properties of boiling citrate solutions. Particularly, Au NSs of 36 and 90 nm diameter were obtained. Au nanoparticles were produced by reducing a 50 mL 0.2 mM chloroauric acid solution ($HAuCl_4$) with the addition of 0.5 mL of a 0.01 M citrate solution under heat and rapid stir for 30 min; 90 nm diameter particles were obtained using 1:0.5 Au/citrate, and 36 nm diameter particles were obtained using a 1:1 Au/citrate ratio. The concentration of the Au nanoparticles was estimated to be around 2 pM, using the experimental extinction intensities at the maximum wavelength, and Mie theory calculations of the extinction cross section for spherical particles with the corresponding diameter (determined by TEM). The morphological characterization of the Au NSs was performed by combining UV–vis spectroscopy, TEM, dynamic light scattering (DLS), and electrodynamic modeling using Mie theory. These results indicate that the average diameter of the Au NSs was 90 and 36 nm, respectively, with a picomolar concentration of 1.32×10^9 NSs/cm^3 (2.44×10^{-12} M).

Partide Funcionalization. EZ-Link biotin-HPDP (*N*-[6-(biotinamido)-hexyl]-3′-(2′-pyridyldithio)propionamide) was used for surface modification of 90 and 36 nm Au NSs. The procedure for the generation of random aggregates consists of incubation for 3 h at room temperature of a 30 mL NS solution in the presence of EZ-Link biotin-HPDP (molar ratio NSs/biotin 1:1). In the case of the generation of dimeric structures, 30 mL NS solution was incubated simultaneously with EZ-Link biotin-HPDP and with streptavidin (STV) (molar ratio NSs/biotin/STV 1:1:0.5) for 3 h at room temperature.

In all cases, biotin was "activated" by previous reaction with mercaptoundecanoic acid (MUA), with a 1:10 biotin/MUA ratio.

Extinction Measurements. The characterization by UV–vis spectroscopy was carried out scanning in the 200–1100 nm range. The spectra were measured using a Shimazdu UV-1700 PharmaSpec spectrophotometer with a 1 cm quartz cell at room temperature.

DLS Measurements. The characterization by dynamic light scattering (DLS) was performed by recording the intensity of the scattered light as a function of the particle diameter in colloidal solutions. The samples were measured using a Delsa Nano 2.2 spectrometer with a 1 cm quartz cell at room temperature.

Electron Microscopy. Transmission electron microscopy (TEM) images were obtained using a JEM-JEOL 1120 EXII under an accelerating voltage of 80 kV. Samples were prepared by adding one drop (~50 μL) of the sample colloidal solution onto a holey carbon/Formvar-coated copper TEM grid (100 mesh).

SERS Measurements. SERS measurements were performed using a Horiba LabRaman confocal microscope with a 5× (NA = 0.12) objective in the backscattering geometry. The spectra acquisition time was 20 s with a 600 lines mm^{-1} grating, giving a resolution of 4 cm^{-1}. The excitation wavelengths used were 514 and 633 nm (laser lines from argon and He–Ne, respectively). All measurements were performed at room temperature and were calibrated to Si and to H_2O bands in the colloidal solutions.

Computational Methods. The optical response of Au NS random aggregates and dimers was computed using the generalized multiparticle Mie (GMM) theory. In all near-field calculations presented in this work, the direction of the incident wavevector k is perpendicular to the line that connects the sphere centers (dimer axis), and the dielectric function tabulated by Palik for Au was employed.[61] For each dimer analyzed, the separation parameter between the nanospheres is large enough so that nonlocal effects on the dielectric constant can be neglected. For the calculations of the cluster near-field properties, we used a multipolar order of 14, while for all other calculations, a multipolar order of 35 was used. For the simulation of the extinction of the dimers in solution, the spectra were averaged over 8 different orientations.

Conflict of Interest: The authors declare no competing financial interest.

Acknowledgment. Prof. Dr. Alfredo Cáceres and Prof. Dr. Jorge Romero are acknowledged for supplying biological samples. We also thank Dr. Claudia Nome for her technical assistance in TEM. Authors also acknowledge financial support of CONICET, SECYT-UNC, and PME 2006−1544.

Supporting Information Available: Optical and morphological characterization of Au nanospheres; optical and morphological characterization, near-field calculations, and optical response of 36 nm Au NS substrates. This material is available free of charge *via* the Internet at http://pubs.acs.org.

REFERENCES AND NOTES

1. Kelly, K. L.; Coronado, E. A.; Zhao, L. L.; Schatz, G. C. The Optical Properties of Metal Nanoparticles: The Influence of Size, Shape, and Dielectric Environment. *J. Phys. Chem. B* **2003**, *107*, 668–677.
2. Perassi, E. M.; Hernandez-Garriddo, J. C.; Moreno, M. S.; Encina, E. R.; Coronado, E. A.; Midgley, P. A. Using Highly Accurate 3D Nanometrology To Model the Optical Properties of Highly Irregular Nanoparticles: A Powerful Tool for Rational Design of Plasmonic Devices. *Nano Lett.* **2010**, *10*, 2097–2104.
3. Kambhampati, P.; Child, C. M.; Foster, M. C.; Campion, A. On the Chemical Mechanism of Surface Enhanced Raman Scattering: Experiment and Theory. *J. Chem. Phys.* **1998**, *108*, 5013–5026.
4. Li, S.; Pedano, M. L.; Chang, S.-H.; Mirkin, C. A.; Schatz, G. C. Gap Structure Effects on Surface-Enhanced Raman Scattering Intensities for Gold Gapped Rods. *Nano Lett.* **2010**, *10*, 1722–1727.
5. Su, K. H.; Wei, Q. H.; Zhang, X.; Mock, J. J.; Smith, D. R.; Schultz, S. Interparticle Coupling Effects on Plasmon Resonances of Nanogold Particles. *Nano Lett.* **2003**, *3*, 1087–1090.
6. Jiang, J.; Bosnick, K.; Maillard, M.; Brus, L. Single Molecule Raman Spectroscopy at the Junctions of Large Ag Nanocrystals. *J. Phys. Chem. B* **2003**, *107*, 9964–9972.
7. Gunnarsson, L.; Bjerneld, E. J.; Xu, H.; Petronis, S.; Kasemo, B.; Kall, M. Interparticle Coupling Effects in Nanofabricated Substrates for Surface-Enhanced Raman Scattering. *Appl. Phys. Lett.* **2001**, *78*, 802–804.
8. Jain, P. K.; El-Sayed, M. A. Surface Plasmon Coupling and Its Universal Size Scaling in Metal Nanostructures of Complex Geometry: Elongated Particle Pairs and Nanosphere Trimers. *J. Phys. Chem. C* **2008**, *112*, 4954–4960.
9. Rechberger, W.; Hohenau, A.; Leitner, A.; Krenn, J. R.; Lamprecht, B.; Aussenegg, F. R. Optical Properties of Two Interacting Gold Nanoparticles. *Opt. Commun.* **2003**, *220*, 137–141.
10. Xu, H. X.; Aizpurua, J.; Kall, M.; Apell, P. Electromagnetic Contributions to Single-Molecule Sensitivity in Surface-Enhanced Raman Scattering. *Phys. Rev. E* **2000**, *62*, 4318–4324.
11. Schwartzberg, A. M.; Grant, C. D.; Wolcott, A.; Talley, C. E.; Huser, T. R.; Bogomolni, R.; Zhang, J. Z. Unique Gold Nanoparticle Aggregates as a Highly Active Surface-Enhanced Raman Scattering Substrate. *J. Phys. Chem. B* **2004**, *108*, 19191–19197.
12. Hao, E.; Schatz, G. C. Electromagnetic Fields around Silver Nanoparticles and Dimers. *J. Chem. Phys.* **2004**, *120*, 357–366.
13. Kneipp, K.; Wang, Y.; Kneipp, H.; Perelman, L. T.; Itzkan, I.; Dasari, R. R.; Feld, M. S. Single Molecule Detection Using Surface-Enhanced Raman Scattering (SERS). *Phys. Rev. Lett.* **1997**, *78*, 1667–1670.
14. Sztainbuch, I. W. The Effects of Au Aggregate Morphology on Surface-Enhanced Raman Scattering Enhancement. *J. Chem. Phys.* **2006**, *125*, 124707–124712.
15. Le Ru, E. C.; Etchegoin, P. G. Sub-Wavelength Localization of Hot-Spots in SERS. *Chem. Phys. Lett.* **2004**, *396*, 393–397.
16. Rodriguez-Lorenzo, L.; Alvarez-Puebla, R. A.; Pastoriza-Santos, I.; Mazzucco, S.; Stephan, O.; Kociak, M.; Liz-Marzan, L. M.; Garcia de Abajo, F. J. Zeptomol Detection through Controlled Ultrasensitive Surface-Enhanced Raman Scattering. *J. Am. Chem. Soc.* **2009**, *131*, 4616–4618.
17. Lim, D.-K.; Jeon, K.-S.; Kim, H. M.; Nam, J.-M.; Suh, Y.-D. Nanogap-Engineerable Raman-Active Nanodumbbells for Single-Molecule Detection. *Nat. Mater.* **2010**, *9*, 60–67.
18. Xu, H.; Bjerneld, E. J.; Kall, M.; Borjesson, L. Spectroscopy of Single Hemoglobin Molecules by Surface Enhanced Raman Scattering. *Phys. Rev. Lett.* **1999**, 4357–4360.
19. Wustholz, K. L.; Henry, A.-L.; McMahon, J. M.; Freeman, R. G.; Valley, N.; Piotti, M. E.; Natan, M. J.; Schatz, G. C.; Van Duyne, R. P. Structure−Activity Relationships in Gold Nanoparticle Dimers and Trimers for Surface-Enhanced Raman Spectroscopy. *J. Am. Chem. Soc.* **2010**, *132*, 10903–10910.
20. Yi, C.; Liu, D.; Yang, M. Building Nanoscale Architectures by Directed Synthesis and Self-Assembly. *Curr. Nanosci.* **2009**, *5*, 75–87.
21. Gregas, M. K.; Scaffidi, J. P.; Lauly, B.; Vo-Dinh, T. Surface-Enhanced Raman Scattering Detection and Tracking of Nanoprobes: Enhanced Uptake and Nuclear Targeting in Single Cells. *Appl. Spectrosc.* **2010**, *8*, 858–866.
22. Wang, J.; Boriskina, S. V.; Wang, H.; Reinhard, B. M. Illuminating Epidermal Growth Factor Receptor Densities on Filopodia through Plasmon Coupling. *ACS Nano* **2011**, *5*, 6619–6628.
23. Hodges, M. D.; Kelly, J. G.; Bentley, A. J.; Fogarty, S.; Patel, I. I.; Martin, F. L.; Fullwood, N. J. Combining Immunolabeling and Surface-Enhanced Raman Spectroscopy on Cell Membranes. *ACS Nano* **2011**, *5*, 9535–9541.
24. Skadtchenko, B. O.; Aroca, R. Surface-Enhanced Raman Scattering of *p*-Nitrothiophenol Molecular Vibrations of Its Silver Salt and the Surface Complex Formed on Silver Islands and Colloids. *Spectrochim. Acta, Part A* **2001**, *57*, 1009–1016.
25. Haynes, C. L.; Yonzon, C. R.; Zhang, X.; Van Duyne, R. P. Surface-Enhanced Raman Sensors: Early History and the Development of Sensors for Quantitative Biowarfare Agent and Glucose Detection. *J. Raman. Spectrosc.* **2005**, *36*, 471–484.
26. Zhang, D.; Neumann, O.; Wang, H.; Yuwono, V. M.; Barhoumi, A.; Perham, M.; Hartgerink, J. D.; Wittung-Stafshede, P.; Halas, N. J. Gold Nanoparticles Can Induce the Formation of Protein-Based Aggregates at Physiological pH. *Nano Lett.* **2009**, *9*, 666–671.
27. Gearheart, L. A.; Ploehn, H. J.; Murphy, C. J. Oligonucleotide Adsorption to Gold Nanoparticles: A Surface-Enhanced Raman Spectroscopy Study of Intrinsically Bent DNA. *J. Phys. Chem. B* **2001**, *105*, 12609–12615.
28. Ni, J.; Lipert, R. J.; Dawson, G. B.; Porter, M. D. Immunoassay Readout Method Using Extrinsic Raman Labels Adsorbed on Immunogold Colloids. *Anal. Chem.* **1999**, *71*, 4903–4908.
29. Cao, Y. C.; Jin, R.; Nam, J. M.; Thaxton, C. S.; Mirkin, C. A. Raman Dye-Labeled Nanoparticle Probes for Proteins. *J. Am. Chem. Soc.* **2003**, *125*, 14676–14677.
30. Su, X.; Zhang, J.; Sun, L.; Koo, T.-W.; Chan, S.; Sundararajan, N.; Yamakawa, M.; Berlin, A. A. Composite Organic−Inorganic Nanoparticles (COINs) with Chemically Encoded Optical Signatures. *Nano Lett.* **2005**, *5*, 49–54.
31. Taylor, R.; Lee, T.; Scherman, O. A.; Esteban, R.; Aizpurua, J.; Huang, F. M.; Baumberg, J. J.; Mahajan, S. Precise Subnanometer Plasmonic Junctions for SERS within Gold Nanoparticle Assemblies Using Cucurbit[n]uril "Glue". *ACS Nano* **2011**, *5*, 3878–3887.
32. Li, W.; Camargo, P. H. C.; Lu, X.; Xia, Y. Dimers of Silver Nanospheres: Facile Synthesis and Their Use as Hot Spots for Surface-Enhanced Raman Scattering. *Nano Lett.* **2009**, *9*, 485–490.
33. Jarvis, R. M.; Rowe, W.; Yaffe, N. R.; O'Conner, R.; Knowles, J. D.; Blanch, E. W.; Goodacre, R. Multiobjective Evolutionary Optimisation for Surface-Enhanced Raman Scattering. *Anal. Bioanal. Chem.* **2010**, *397*, 1893–1901.
34. Connolly, S.; Fitzmaurice, D. Programmed Assembly of Gold Nanocrystals in Aqueous Solution. *Adv. Mater.* **1999**, *11*, 1202–1205.

35. Costanzo, P. J.; Patten, T. E.; Seery, T. A. Protein-Ligand Mediated Aggregation of Nanoparticles: A Study of Synthesis and Assembly Mechanism. *Chem. Mater.* **2004**, *16*, 1775–1785.
36. Caswell, K. K.; Wilson, J. N.; Bunz, U. H. F.; Murphy, C. J. Preferential End-to-End Assembly of Gold Nanorods by Biotin–Streptavidin Connectors. *J. Am. Chem. Soc.* **2003**, *125*, 13914–13915.
37. Gole, A.; Murphy, C. J. Biotin–Streptavidin-Induced Aggregation of Gold Nanorods: Tuning Rod–Rod Orientation. *Langmuir* **2005**, *21*, 10756–10762.
38. Lee, J.; Govorov, A. O.; Dulka, J.; Kotov, N. A. Bioconjugates of CdTe Nanowires and Au Nanoparticles: Plasmon–Exciton Interactions, Luminescence Enhancement, and Collective Effects. *Nano Lett.* **2004**, *4*, 2323–2330.
39. Li, M.; Dujardin, E.; Mann, S. Programmed Assembly of Multi-layered Protein/Nanoparticle–Carbon Nanotube Conjugates. *Chem. Commun.* **2005**, 4952–4954.
40. Lee, J.; Govorov, A. O.; Kotov, N. A. Induction of Cell Polarization and Migration by a Gradient of Nanoscale Variations in Adhesive Ligand Spacing. *Nano Lett.* **2005**, *5*, 2063–2069.
41. Wang, S. P.; Mamedova, N.; Kotov, N. A.; Chen, W.; Studer, J. Antigen/Antibody Immunocomplex from CdTe Nanoparticle Bioconjugates. *Nano Lett.* **2002**, *2*, 817–822.
42. Wang, Y.; Tang, Z. Y.; Tan, S. S.; Kotov, N. A. Biological Assembly of Nanocircuit Prototypes from Protein-Modified CdTe Nanowires. *Nano Lett.* **2005**, *5*, 243–248.
43. Chang, J. Y.; Wu, H. M.; Chen, H.; Ling, Y. C.; Tan, W. H. Oriented Assembly of Au Nanorods Using Biorecognition System. *Chem. Commun.* **2005**, 1092–1094.
44. Shenton, W.; Davis, S. A.; Mann, S. Directed Self-Assembly of Nanoparticles into Macroscopic Materials Using Antibody–Antigen Recognition. *Adv. Mater.* **1999**, *11*, 449–452.
45. Hiddessen, A. L.; Rodgers, S. D.; Weitz, D. A.; Hammer, D. A. Assembly of Binary Colloidal Structures *via* Specific Biological Adhesion. *Langmuir* **2000**, *16*, 9744–9753.
46. Stevens, M. M.; Flynn, N. T.; Wang, C.; Tirrell, D. A.; Langer, R. Coiled-Coil Peptide-Based Assembly of Gold Nanoparticles. *Adv. Mater.* **2004**, *16*, 915–918.
47. Xu, L.; Guo, Y.; Xie, R. G.; Zhuang, J. Q.; Yang, W. S.; Li, T. J. Three-Dimensional Assembly of Au Nanoparticles Using Dipeptides. *Nanotechnology* **2002**, *13*, 725–728.
48. Galarreta, B. C.; Norton, P. R.; Lagugne-Labarthet, F. SERS Detection of Streptavidin/Biotin Monolayer Assemblies. *Langmuir* **2011**, *27*, 1494–1498.
49. Chirra, H. D.; Sexton, T.; Biswal, D.; Hersh, L. B.; Hilt, J. Z. Catalase-Coupled Gold Nanoparticles: Comparison between the Carbodiimide and Biotin–Streptavidin Methods. *Acta Biomater.* **2011**, *7*, 2865–2872.
50. Encina, E. R.; Coronado, E. A. On the Far Field Optical Properties of Ag–Au Nanosphere Pairs. *J. Phys. Chem. C* **2010**, *114*, 16278–16284.
51. Encina, E. R.; Coronado, E. A. Plasmon Coupling in Silver Nanosphere Pairs. *J. Phys. Chem. C* **2010**, *114*, 3918–3923.
52. Encina, E. R.; Coronado, E. A. Near Field Enhancement in Ag Au Nanospheres Heterodimers. *J. Phys. Chem. C* **2011**, *115*, 15908–15914.
53. Coronado, E. A.; Encina, E. R.; Stefani, F. D. Optical Properties of Metallic Nanoparticles: Manipulating Light, Heat and Forces at the Nanoscale. *Nanoscale* **2011**, *3*, 4042–4059.
54. Marhaba, S.; Bachelier, G.; Bonnet, C.; Broyer, M.; Cottancin, E.; Grillet, N.; Lermé, J.; Vialle, J.-L.; Pellarin, M. Surface Plasmon Resonance of Single Gold Nanodimers near the Conductive Contact Limit. *J. Phys. Chem. C* **2009**, *113*, 4349–4356.
55. Park, S.-J.; Lazarides, A. A.; Storhoff, J. J.; Pesce, L.; Mirkin, C. A. The Structural Characterization of Oligonucleotide-Modified Gold Nanoparticle Networks Formed by DNA Hybridization. *J. Phys. Chem. B* **2004**, *108*, 12375–12380.
56. Srisa-Art, M.; Dyson, E. C.; de Mello, A. J.; Edel, J. B. Monitoring of Real-Time Streptavidin–Biotin Binding Kinetics Using Droplet Microfluidics. *Anal. Chem.* **2008**, *80*, 7063–7067.
57. Zuloaga, J.; Nordlander, P. On the Energy Shift between Near-Field and Far-Field Peak Intensities in Localized Plasmon Systems. *Nano Lett.* **2011**, *11*, 1280–1283.
58. Le Ru, E. C.; Blackie, E.; Meyer, M.; Etchegoin, P. G. Surface Enhanced Raman Scattering Enhancement Factors: A Comprehensive Study. *J. Phys. Chem. C* **2007**, *111*, 13794–13803.
59. Le Ru, E.; Etchegoin, P. G. *Principles of Surface Enhanced Raman Spectroscopy*; Elsevier: Amsterdam, 2009; Vol. 1.
60. Kang, T.; Yoon, I.; Kim, J.; Ihee, H.; Kim, B. Au Nanowire–Au Nanoparticles Conjugated System which Provides Micrometer Size Molecular Sensors. *Chem.—Eur. J.* **2010**, *16*, 1351–1355.
61. Palik, E. D. Handbook of Optical Constants of Solids; Academic Press: New York, 1985.